NANO · MICRO small

Supporting Information

for *Small*, DOI 10.1002/smll.202308282

Extending Cycling Life Beyond 300 000 Cycles in Aqueous Zinc Ion Capacitors Through Additive Interface Engineering

Wenchao Shi, Zhenjun Song, Weiyi Sun, Yu Liu, Yalong Jiang, Qi Li and Qinyou An**

Supporting Information

Extending Cycling Life beyond 300,000 Cycles in Aqueous Zinc Ion Capacitors through Additive Interface Engineering

Wenchao Shi [a], Zhenjun Song [b], Weiyi Sun [a], Yu Liu [a], Yalong Jiang [c], Qi Li [d] and Qinyou An [a]**

[a]State Key Laboratory of Advanced Technology for Materials Synthesis and Processing, Wuhan University of Technology, Wuhan, 430070, P. R. China

[b]School of Pharmaceutical and Materials Engineering, Taizhou University, Taizhou, 318000, P. R. China

[c]State Key Laboratory of New Textile Materials and Advanced Processing Technologies, Wuhan Textile University, Wuhan, 430200, China

[d]National energy key laboratory for new hydrogen-ammonia energy technologies, Foshan Xianhu Laboratory, Foshan 528200, P.R. China.

Corresponding Author

*E-mail: liqi1@xhlab.cn; anqinyou86@whut.edu.cn

Experimental.

Electrolyte Preparation:

The 2 M $ZnSO_4$ electrolyte was prepared by dissolving $ZnSO_4 \cdot 7H_2O$ in deionized water. The subject electrolytes were prepared by adding different amounts of dibenzenesulfonimide (BBI) (Aladdin, >97%) into 2 M $ZnSO_4$ electrolyte, noted as BBI/$ZnSO_4$. The optimized concentration of BBI was 0.25 g L^{-1}.

Fabrication of Active Carbon Cathode Material:

Active carbon (AC) was synthesized from phenol resin through a multi-step process. Initially, phenol resin was mixed with deionized water (DI water) at a temperature of 75 °C and stirred for 2 hours. The resulting mixture was then transferred into a 100 ml autoclave and heated at 180 °C for 12 hours. After centrifugation and drying, the obtained precipitates were collected. Subsequently, the collected sample underwent pre-carbonization at a temperature of 600 °C for 1 hour under N_2 flow. The carbon precursor was then mixed with KOH, with KOH/precursor mass ratios of 6, and the resulting mixture was heat-treated under N_2 flow at a temperature of 800 °C for 1 hour. Finally, the products were obtained by washing them with HCl solution and DI water, resulting in the synthesis of AC.

Material characterization:

The crystal structures of the materials were analyzed using a D8 Advance X-ray diffractometer with Cu Kα radiation (λ=1.5406 Å). The samples were also subjected to field-emission scanning electron microscopy (FESEM) using a 2020 JEOL-7100F scanning electron microscope. Raman spectra and attenuated total reflection Fourier transform infrared (ATR-FTIR) spectra were recorded using a micro-Raman spectroscopy system (Renishaw INVIA). Nuclear magnetic resonance (NMR) spectra were obtained on a Bruker Avance II 300MHz NMR spectrometer. Additionally, X-ray photoelectron spectroscopy (XPS) results were obtained through a VG MultiLab 2000 instrument. Transmission electron microscopy (TEM), high-resolution TEM, and the energy dispersive X-ray spectroscopy (EDS) mapping were performed on a JEM-2100F transmission electron microscope at 200 kV.

Electrochemical characterization:

The electrochemical workstation (CHI660E, China) was used to test the linear polarization curves between -1.2 and -0.8 V at 5 mV s^{-1}, with Zn foil as the working electrode and counter electrode, and a saturated calomel electrode (SCE) as the reference electrode. The chronoamperometry (CA) curves were measured at an overpotential of -150 mV. The differential capacitance curves were measured by scanning between 0 and 1.0 V at 1000 Hz. For the Zn||Zn symmetrical cells, the Zn foil (100 μm) was cut into a round disk with a

diameter of 10 mm. For the Zn||Cu or Zn||Ti asymmetrical cell, the Cu or Ti foil (100 μm) was cut into a round disk with a diameter of 16 mm. To prepare the AC cathodes, a slurry made up of AC, carbon black (Super P), and polytetrafluoroethylene (PTFE) at a weight ratio of 8:1:1 was pressed onto titanium mesh. The full cells were assembled with the Zn foil anodes (diameter of 12 mm) and AC cathodes separated by a glass fiber separator with a diameter of 17 mm. All cells were assembled as CR2016 coin cells in an air atmosphere. The cycling performances of the cells were measured by the LAND instrument in the voltage range of 0.2 - 1.8 V. Additionally, cyclic voltammetry (CV) was performed with a voltage range of 0.2 - 1.8 V at different scan rates of 1, 2, 5, 8, 10, 20, 30, and 50 mV s^{-1}, and electrochemical impedance spectroscopy (EIS) tests were conducted using an Autolab PGSTAT 302N in a frequency range of 0.01 Hz - 100 kHz.

Calculation method:

We employed dispersion-corrected density-functional theory (DFT-D3) [1] and the plane-wave method to compute the structures and energetics. The projector-augmented-wave (PAW) [2] method in conjunction with the generalized gradient approximation (GGA) was used to determine the dispersion forces and energy. Perdew-Burke-Ernzerhof functional implemented in Vienna Ab Initio Simulation Package (VASP) [3] was adopted to compute the exchange-correlation potentials.

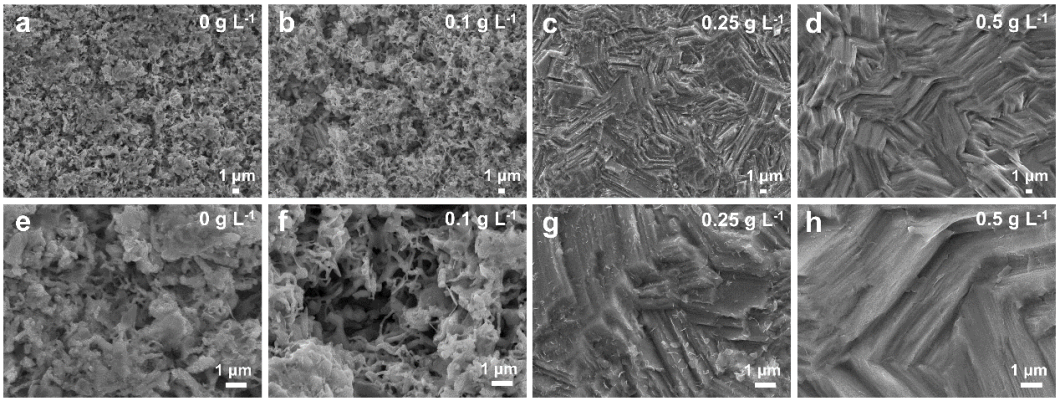

Figure S1. SEM images of Zn deposition layers at different concentrations of BBI additives in beaker batteries under 10 mA cm^{-2} and 5 mAh cm^{-2}, a) 0 g L^{-1}, b) 0.1 g L^{-1}, c) 0.25 g L^{-1}, d) 0.5 g L^{-1}.

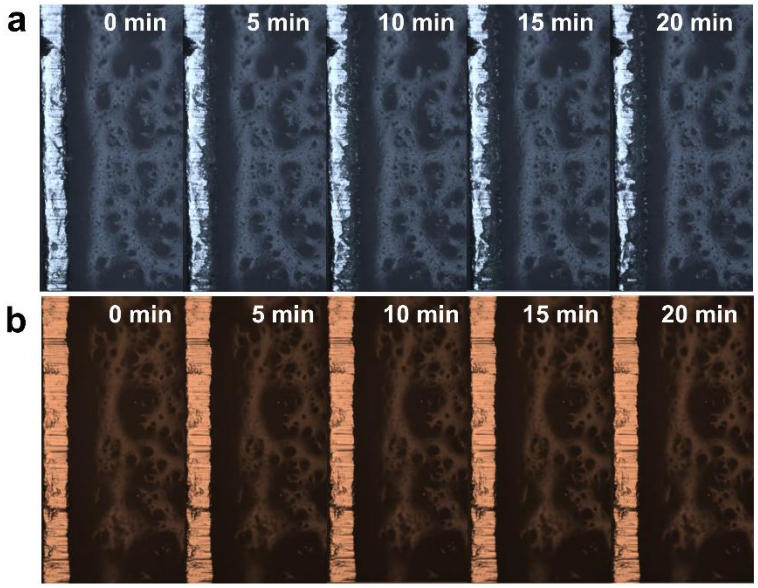

Figure S2. In-situ Zn deposition images on the anode side in Zn||Zn symmetric cells at a current of 5 mA cm^{-2} under a) $ZnSO_4$ and b) BBI/$ZnSO_4$ electrolyte through an optical microscopy system.

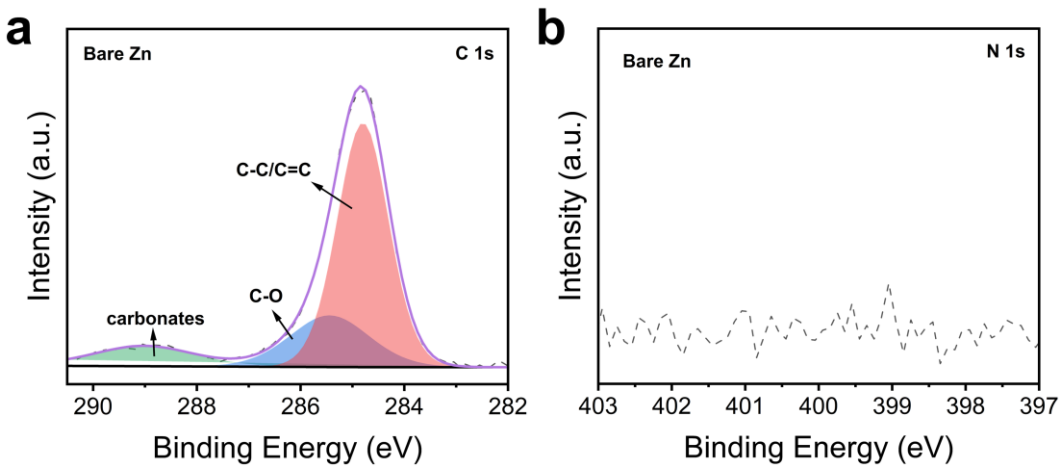

Figure S3. a) C 1s, b) N 1s of bare Zn metal before immersion.

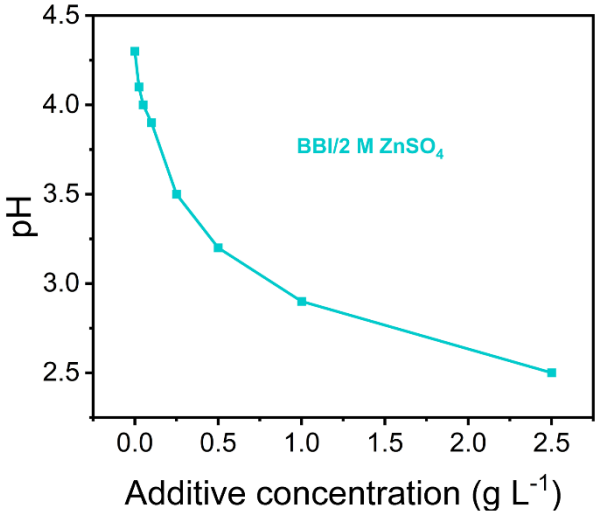

Figure S4. The pH values of different additive concentrations of BBI/$ZnSO_4$ electrolyte.

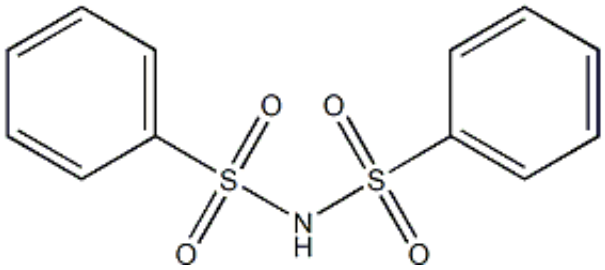

Figure S5. The chemical formula of the BBI molecule.

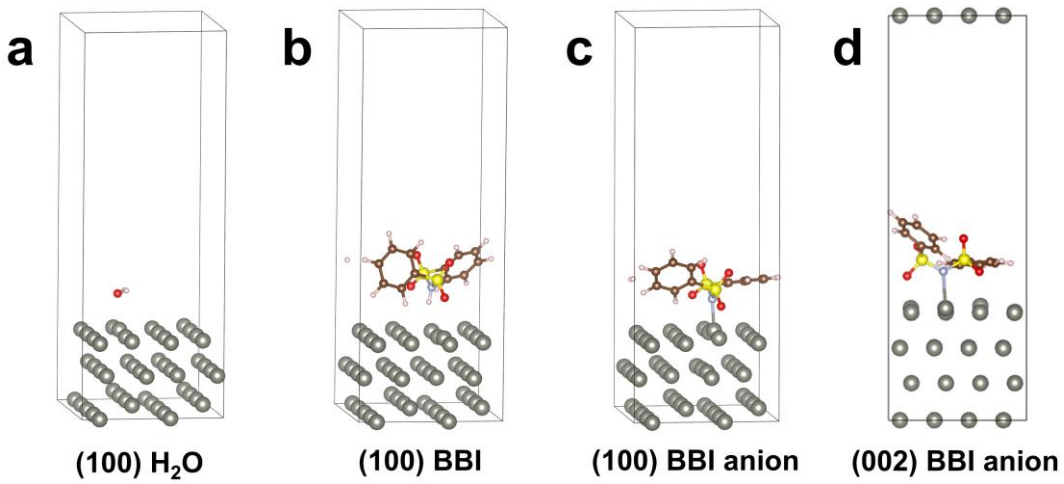

Figure S6. Geometric models of a) water, b) BBI molecule, c) BBI anion absorbed on Zn (100) surface and d) BBI anion absorbed on Zn (002) surface.

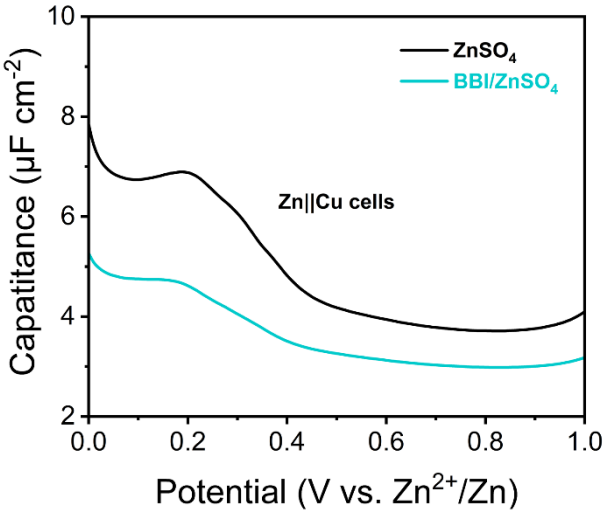

Figure S7. The differential capacitance curves of Zn||Cu cells in $BBI/ZnSO_4$ and $ZnSO_4$ electrolytes.

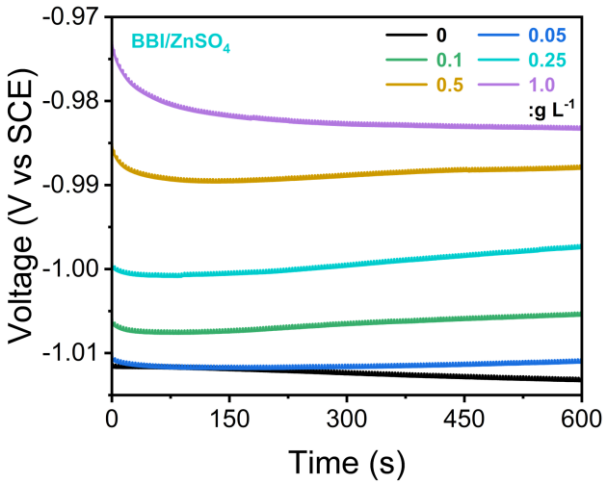

Figure S8. OCP values versus immersion time in BBI/$ZnSO_4$ electrolytes with different additive concentrations.

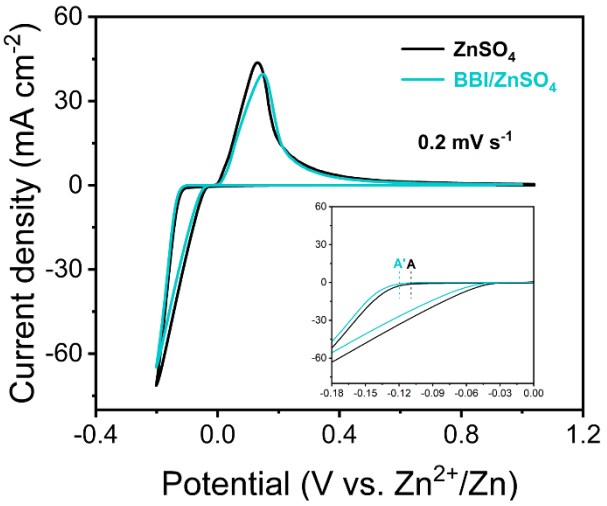

Figure S9. The CV curves of Zn||Ti cells at a scan rate of 0.2 mV s^{-1} in $ZnSO_4$ and BBI/$ZnSO_4$ electrolyte.

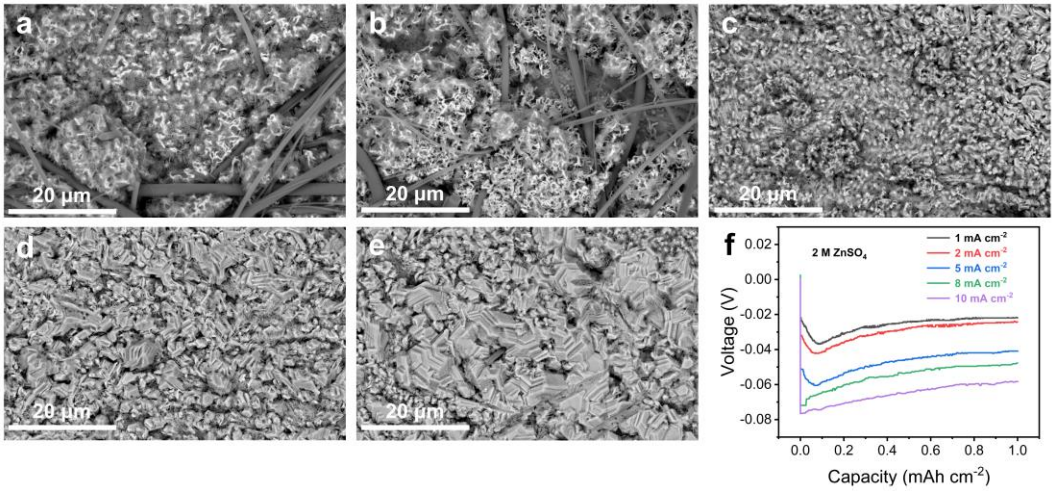

Figure S10. SEM images of Zn deposition layers at different current densities in $ZnSO_4$ electrolyte under 1 mAh^{-2}, a) 1 mA cm^{-2}, b) 2 mA cm^{-2}, c) 5 mA cm^{-2}, d) 8 mA cm^{-2}.e) 10 mA cm^{-2} and f) corresponding deposition curves.

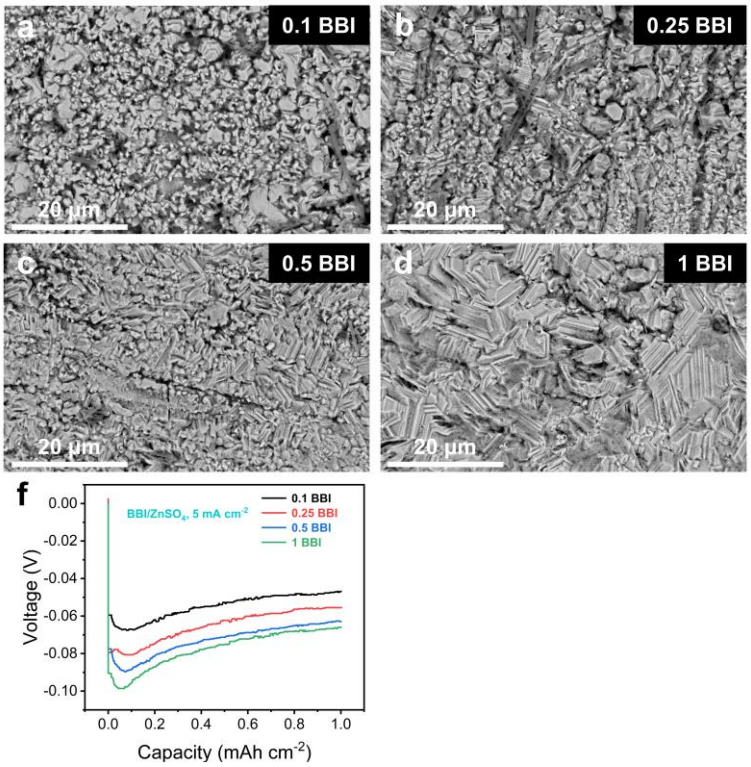

Figure S11. SEM images of Zn deposition layers at different concentrations of BBI additives under 5 mA cm^{-2} and 1 mAh cm^{-2} , a) 0 g L^{-1}, b) 0.1 g L^{-1}, c) 0.25 g L^{-1}, d) 0.5 g L^{-1}, e) 1 g L^{-1} and f) corresponding deposition curves.

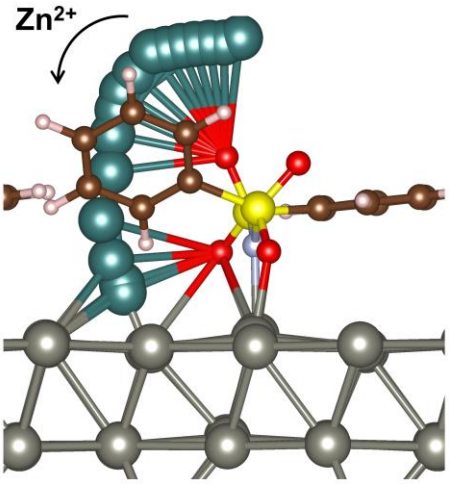

Figure S12. First-principles calculations of the optimum Zn^{2+} diffusion pathway in the BBI-Zn interfacial layer.

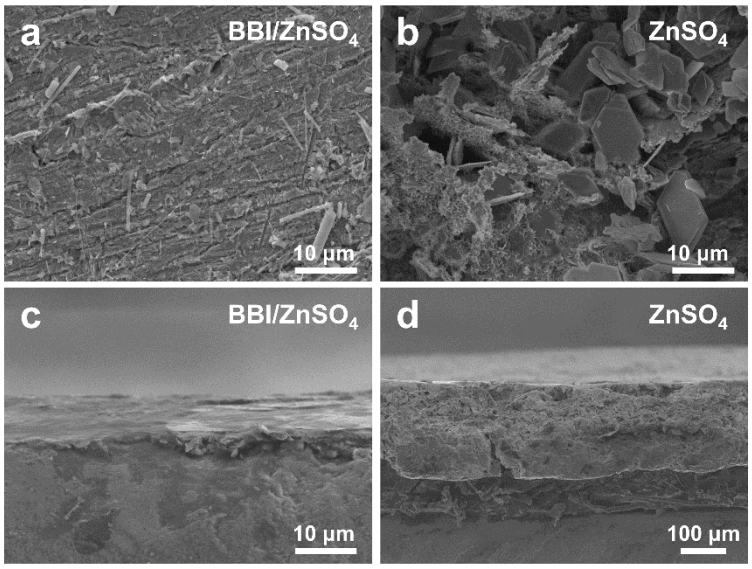

Figure S13. Frontal and cross-sectional SEM images of Zn anodes after 50 cycles in a, c) $BBI/ZnSO_4$ and b, d) $ZnSO_4$ electrolyte at 1 mA cm^{-2} and 0.5 mAh cm^{-2}.

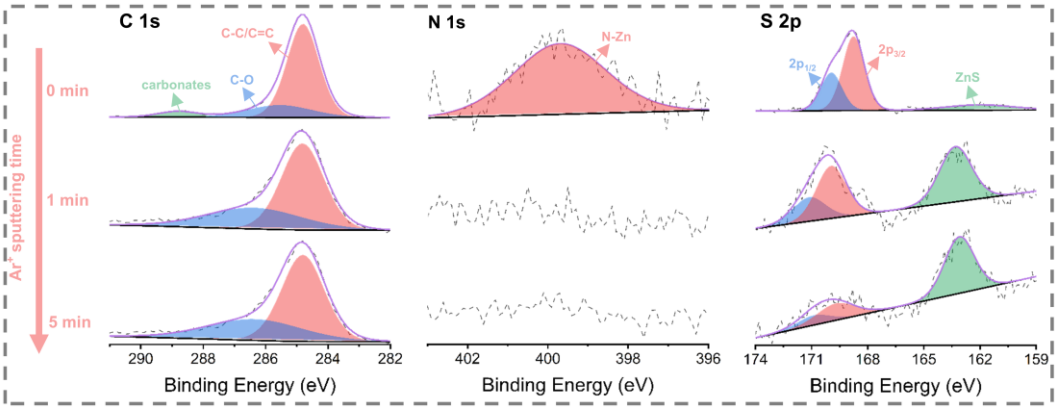

Figure S14. The XPS depth profile for C 1s, N 1s and S 2p of Zn anode surface tested in $BBI/ZnSO_4$ electrolyte for 50 cycles.

Through XPS etching analysis, it was speculated that the possible decomposition equation of the BBI-Zn interfacial layer was as follows:

$$C_6H_5SO_2NSO_2C_6H_5^- \xrightarrow{+xe^-,yH^+} 2C_6H_6 + NH_3 + 2SO_2$$

$$SO_2 + 2Zn^{2+} + 2H^+ + 6e^- \rightarrow ZnS + ZnSO_3 + H_2O$$

The first step involved the decomposition of the BBI anion to produce SO_2, benzene, NH_3, or other analogs under the synergistic action of the enriched electrons on the Zn anode surface and the interfacial hydrogen ions. SO_2 was subsequently reacted with H_2O and Zn^{2+} to form ZnS and $ZnSO_3$.

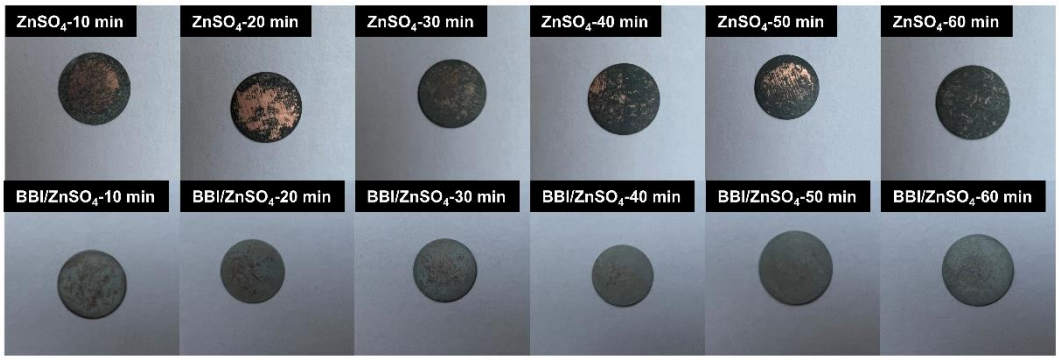

Figure S15. The optical photographs of Zn deposition layers on Cu electrodes with different deposition times at 10 mA cm^{-2} in $ZnSO_4$ and BBI/$ZnSO_4$ electrolytes.

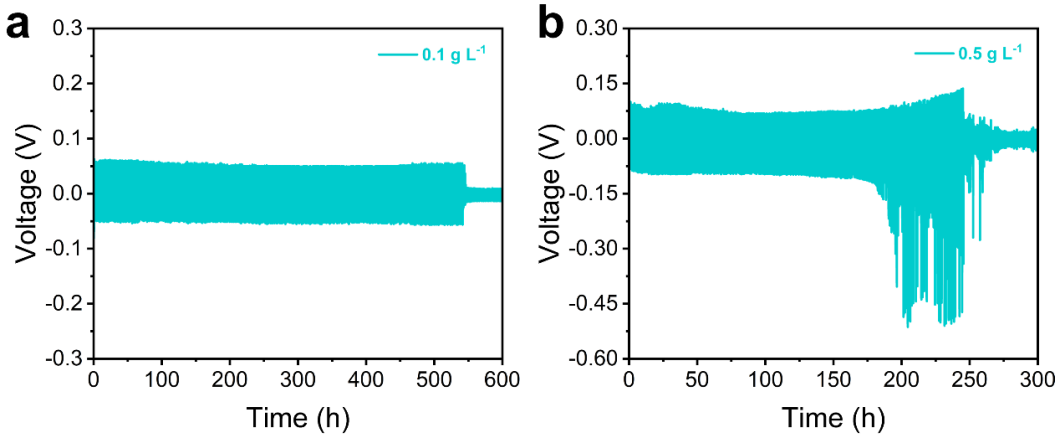

Figure S16. Galvanostatic cycling performance of Zn||Zn cells in a) 0.1 g L^{-1} and b) 0.5 g L^{-1} BBI/$ZnSO_4$ electrolyte at 10 mA cm^{-2}/5 mAh cm^{-2}.

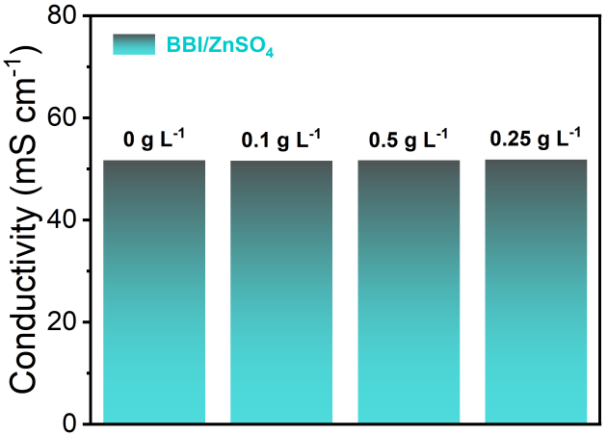

Figure S17. The ion conductivity of electrolyte with different concentration of BBI.

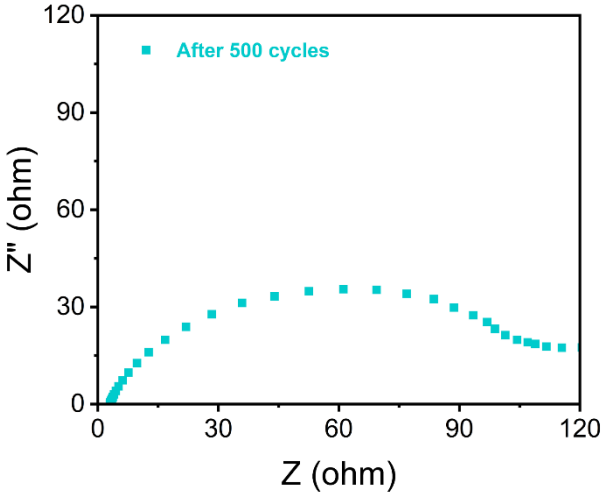

Figure S18. EIS pattern of Zn||Zn cell after 500 cycles in BBI/$ZnSO_4$ electrolyte at 1 mA cm^{-2}/0.5 mAh cm^{-2}.

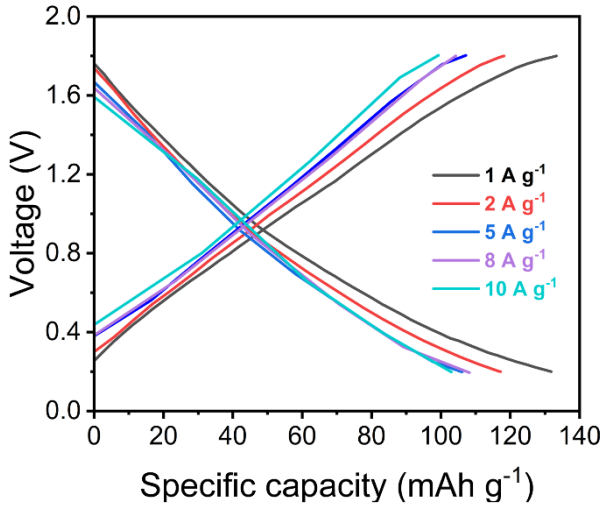

Figure S19. Charge-discharge curves of Zn||AC cell at different current densities.

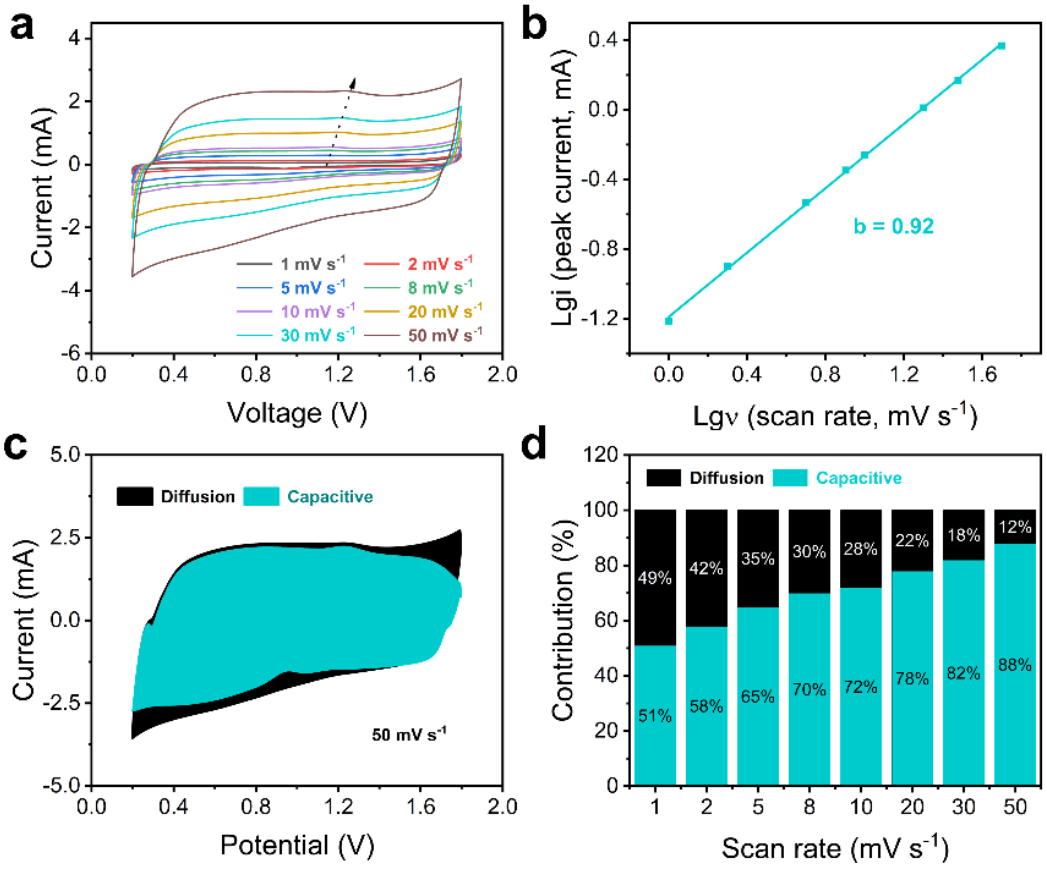

Figure S20. a) CV curves at different scan rates and b) corresponding b values of the oxidation peak. c) The separation of the capacitive and diffusion currents in Zn||AC cell at a scan rate of 50 mV s^{-1}. d) The percentage of capacitive contribution at different scan rates.

It is generally believed that the peak currents (i_p) and scan rates (v) in the CV tests follow the formula: $i_p = av^b (\text{or } \lg i_p = \lg a + b \lg v)$, where a is a constant and b are considered to be the slope of the fitting line. When the b value approaches 0.5, it represents the diffusion-controlled lithium storage process, while when the b value approaches 1.0, it represents the capacitive-controlled process. CV curves of Zn||AC cells at various scan rates were investigated (Figure S20a). The b value of Zn||AC cell at the chosen peak confirmed that the pseudo-capacitance contribution (Figure S20b). The capacitive attribution was assessed to be ≈88% at a scan rate of 50 mV s^{-1} as exhibited in the shadow region (Figure S20c). Moreover, the capacitive contribution of Zn||AC increased with scan rates increasing (Figure S20d).

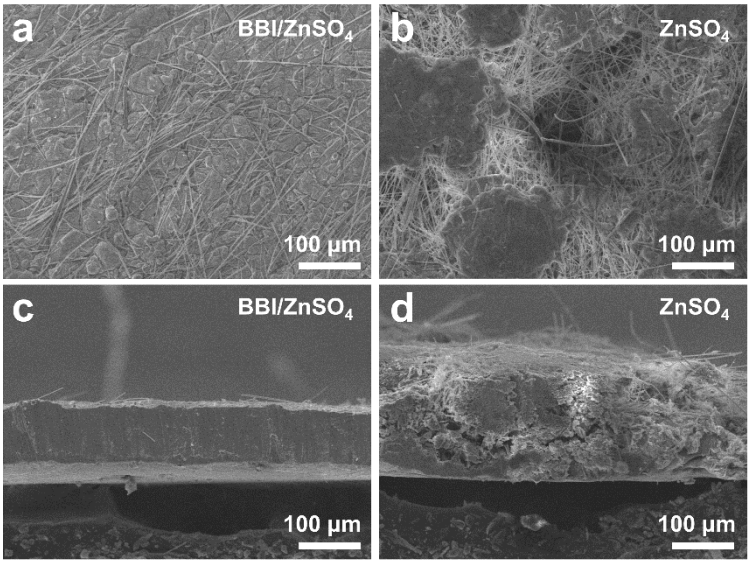

Figure S21. Frontal and cross-sectional SEM images of Zn anodes in a, c) BBI/$ZnSO_4$ after 100,000 cycles and b, d) $ZnSO_4$ electrolyte after 10,000 cycles.

References

[1] a) S. Grimme, J. Antony, S. Ehrlich, H. Krieg, *J. Chem. Phys.* **2010**, 132, 154104; b) S. Grimme, S. Ehrlich, L. Goerigk, *J. Comput. Chem.* **2011**, 32, 1456.

[2] a) P. E. Blochl, *Phys. Rev., B Condens. Matter* **1994**, 50, 17953; b) G. Kresse, D. Joubert, *Phys. Rev. B* **1999**, 59, 1758.

[3] a) K. G, F. J, *Comput. Mater. Sci.* **1996**, 6, 15; b) K. G, F. l. J, *Phys. Rev. B* **1996**, 54, 11169; c) G. Kresse, J. Hafner, *Phys. Rev., B Condens. Matter* **1993**, 47, 558; d) G. Kresse, J. Hafner, *Phys. Rev., B Condens. Matter* **1994**, 49, 14251.